

1 The Temporal Rich Club Phenomenon

2 **Nicola Pedreschi^{1,2}, Demian Battaglia^{2,3}, and Alain Barrat^{1,4}**

3 ¹Aix Marseille Univ, Université de Toulon, CNRS, CPT, Turing Center for Living Systems, Marseille, France

4 ²Aix-Marseille Univ, Inserm, INS, Institut de Neurosciences des Systèmes, Turing Center for Living Systems,
5 Marseille, France

6 ³University of Strasbourg Institute for Advanced Studies (USIAS), Strasbourg, France

7 ⁴Tokyo Tech World Research Hub Initiative (WRHI), Tokyo Institute of Technology, Tokyo, Japan

8 **ABSTRACT**

Identifying the hidden organizational principles and relevant structures of networks representing complex physical systems is fundamental to understand their properties. To this aim, uncovering the structures involving the prominent nodes in a network is an effective approach. In temporal networks, the simultaneity of connections is crucial for temporally stable structures to arise. We thus propose here a novel
9 measure to quantitatively investigate the tendency of well connected nodes to form simultaneous and stable structures in a temporal network. We refer to this tendency, when observed, as the "temporal rich club phenomenon". We illustrate the interest of this concept by analyzing diverse data sets under this lens, and showing how it enables a new perspective on their temporal patterns, from the role of cohesive structures in relation to processes unfolding on top of the network to the study of specific moments of interest in the evolution of the network.

10 **1 Introduction**

11 A wide range of natural, technological and social systems can be represented as networks of agents (nodes)
12 and their interactions (edges)¹⁻³. Typical examples include communication systems⁴, transportation
13 infrastructures⁵, biological and ecological systems⁶⁻⁸, brain networks⁹ or social interactions¹⁰⁻¹². Such
14 representation offers a common framework and common tools to analyse these systems, link their structure
15 and dynamics and investigate processes on top of them. In particular, a common challenge consists in
16 identifying relevant network structures, and several complementary approaches have been put forward to

17 characterize networked data sets and their more central elements. For instance, hubs, single nodes with very
18 large numbers of connections (degrees), are known to influence spreading processes^{1,3}. A quantification of
19 a core-periphery structure identifies a central core of well-connected nodes¹³. The k-core decomposition¹⁴
20 decomposes the network into subgraphs of increasing connectedness, with correspondingly increasing
21 influence in spreading processes¹⁵. The rich-club coefficient quantifies whether the nodes with large
22 numbers of neighbors (the hubs) tend to form more tightly interconnected groups^{16–20} that can, for instance,
23 share the control of resources in social and collaboration networks¹⁸, or shape the routing and integration
24 of communication in brain networks^{21–23}.

25 While these approaches are effective for static networks, an increasing number of data sets
26 include temporal information about edges, which appear and disappear on different time scales: static
27 networks are often only aggregated representations of the resulting temporal networks^{24–26}. Thus, any
28 structure found in a static network obtained by temporal aggregation of data could in fact be formed by
29 edges that were active at unrelated times^{27,28}. To investigate structures in temporal networks, it is crucial
30 to take into account the complex temporal properties of the data, as already argued in early works on
31 temporal networks^{27,28}. For instance, a static hub might have drastically different numbers of neighbors at
32 different times^{27,28}, as well as different dynamical properties^{27–29}; Network modular structures can evolve
33 (which can e.g. be a resource for cognitive processing³⁰); Processes can only take causal, time respecting
34 paths among the elements of a network^{31,32}; Concurrency, i.e., the simultaneity of connections of a given
35 node with others, is key in epidemic propagation processes^{28,33}; Dynamic or temporal motifs can be
36 defined as the repetition over time of simultaneous subgraphs²⁸ or as the repetition of the connections in a
37 small temporal subgraph in a given order^{34–36}; Well connected structures such as cores are not static but
38 are defined on specific time-intervals^{37,38}.

39 Overall, structures and hierarchies in temporal networks need to be defined and investigated
40 taking into account (i) the temporality and simultaneity of the interactions forming the structure, (ii)
41 the time-span on which the structure exists. Here, we propose a new way to investigate the cohesion
42 of increasingly central nodes in a temporal network, namely, the temporal rich club (TRC) coefficient:
43 given a temporal network, our aim is to quantify whether nodes who interact with increasing numbers of
44 other nodes (i.e., with increasing degree in the aggregate network) tend also to interact with each other
45 simultaneously and in a stable way. We thus first define the Δ -cohesion of a group of nodes at each time
46 t , as the density of links persistently connecting the nodes in the group during a time interval of length

Δ starting at t . We then consider groups of nodes of increasing degree in the aggregated network, and measure the maximum value of their Δ -cohesion over time: this quantifies whether these groups are tightly and simultaneously interconnected for a certain duration Δ .

Moreover, and as in the case of the static rich club coefficient^{17,39}, a natural question is whether the simultaneous connections between high degree nodes could exist just by chance, so that we compare the result with an adequate null model for temporal networks⁴⁰. To show the broad interest of this new analysis tool for temporal networks, we consider empirical temporal networks representing very different systems: an air transportation infrastructure, face-to-face interaction networks in social contexts, and a network of neurons exchanging information. In each case, we compute the temporal rich-club coefficient for the data and the null model, and highlight how it unveils interesting properties of the data. We show in particular how static and temporal rich clubs are independent phenomena, how a temporal rich club impacts spreading processes, and how a temporal network undergoing successive states⁴¹ can present a distinct temporal rich club in each state, with different temporal patterns despite similar static structures. Our findings suggest that the temporal rich club coefficient provides a new item in the toolbox for the analysis of temporal networks, interlinked with but different from and complementary to the investigation of other types of structures in temporal networks such as stable or unstable hubs²⁷, dynamic motifs^{28,35} or span-cores³⁷ (in the same way as investigating the static rich club is different from showing the existence of hubs, cores or static motifs): for instance, a stable hub might be connected to low-degree nodes, and/or to different nodes at different times, and motifs can involve nodes of different degrees. This new tool can thus shed light on the role and connections of the most prominent elements and provide relevant information on the different periods of interest of the network.

2 Results

2.1 The temporal rich club

We consider a temporal network in discrete time on a time interval $[1, T]$, represented as a series of instantaneous snapshots of the network at each time stamp (Figure 1.a)^{24,27}. We denote by temporal edges the interactions between pairs of nodes in each snapshot. The temporal aggregation over $[1, T]$ yields a static (aggregated) network $G = (V, E)$ with set of nodes V and set of edges E (Figure 1.b), in which an

edge is drawn between two nodes i and j if they have at least shared one temporal edge, with a weight w_{ij} given by the number of temporal edges between i and j . The degree k of a node in G is the number of distinct other nodes with which it has interacted at least once in $[1, T]$, and its strength s the total number of temporal edges it has participated to.

As stated above, our goal is to quantify a temporal rich club effect, i.e., whether nodes of increasing degree in G tend to be more connected than by chance simultaneously and for a certain duration. We first remind that the rich club coefficient was defined for a static network as the density of edges in the subset $S_{>k}$ of the $N_{>k}$ nodes with degree larger than k ^{16,17,39}: $\phi(k) = \frac{2E_{>k}}{N_{>k}(N_{>k}-1)}$, where $E_{>k}$ is the number of edges connecting the $N_{>k}$ nodes. This coefficient quantifies the rich club connectivity: how densely the subset $S_{>k}$ is interconnected. Its evolution with k has been discussed, as an increasing $\phi(k)$ indicates that nodes of larger degree tend to form increasingly connected groups of nodes (the so-called "rich club effect")^{16,17}, while $\phi(k)$ can also collapse to 0 at large k , for instance in very disassortative networks³⁹. Moreover, $\phi(k)$ can be compared with the value $\phi_{ran}(k)$ obtained in an equivalent randomized graph^{17,39}.

Here, to take into account temporality, we first define at each time t the Δ -cohesion. To this aim, we consider the set of ties $E_{>k}(t, \Delta)$ (between the nodes of $S_{>k}$) that remain stable over the time interval $[t, t + \Delta]$ (Figure 1c): the Δ -cohesion $\varepsilon_{>k}(t, \Delta)$ is then the number $|E_{>k}(t, \Delta)|$ of such ties, normalized by its maximal possible value $N_{>k}(N_{>k} - 1)/2$. Note that $\varepsilon_{>k}(t, \Delta = 1)$ is the instantaneous density between the nodes of $S_{>k}$, i.e., a kind of instantaneous static rich-club coefficient calculated with the same ranking of nodes in all snapshots (given by the aggregated degree), which is different from the rich-club coefficient of the instantaneous snapshot at time t computed using the instantaneous values of the degree, as the degree of each node can fluctuate²⁸. We then define the temporal rich club coefficient as the maximal cohesion observed in the temporal network over time:

$$M(k, \Delta) \equiv \max_t \varepsilon_{>k}(t, \Delta) .$$

In other terms, $M(k, \Delta)$ is the maximal density of temporal edges observed in a stable way for a duration Δ among nodes of aggregated degree larger than k : it allows to understand and quantify (i) whether the static rich-club patterns correspond to a structure that actually existed at some instant, with the same density of links measured in the static aggregated network, or with a smaller density, (ii) how stable such structure

92 was, (iii) or whether the static rich-club is actually formed by links that appeared at unrelated times and
 93 never existed in a simultaneous way. While, by definition, $M(k, \Delta)$ is non-increasing as a function of Δ , a
 94 $M(k, \Delta)$ increasing with k denotes that the most connected nodes tend as well to be increasingly connected
 95 with each other in a simultaneous way for a duration at least Δ . We note that, for large k , this is a different
 96 requirement from distinguishing stable and unstable hubs²⁷, even if a stable hub would statistically tend to
 97 contribute to such connectedness. Indeed, $M(k, \Delta)$ focuses on the links between hubs: a hub might have a
 98 consistently large instantaneous degree but towards small degree nodes or towards changing neighbors⁴²,
 99 while another might have a fluctuating degree but still maintain its few links towards other high degree
 100 nodes, hence contributing to a temporal rich club. Moreover, as the simultaneity of connections within
 101 $S_{>k}$ might simply be due to chance, we compare $M(k, \Delta)$ with the value $M_{ran}(k, \Delta)$ obtained in a suitable
 102 null model of the temporal network: $\mu(k, \Delta) \equiv M(k, \Delta)/M_{ran}(k, \Delta) > 1$ indicates that the nodes of degree
 103 larger than k are more connected simultaneously on at least one time interval of duration Δ than expected
 104 by chance, denoting a temporal rich club ordering. Although there is a large variety of null models for
 105 temporal networks⁴⁰, we focus here on the simultaneity of connections: we thus consider a randomization
 106 procedure that preserves the overall activity timeline of the temporal network (number of temporal edges
 107 at each time) as well as the degree of each node and weight of each link (i.e., number of snapshots in which
 108 the link is active) in the aggregated graph. To this aim, we consider the list of all temporal edges, under
 109 the form (i_q, j_q, t_q) denoting an interaction between nodes i_q and j_q at time $t_q \in [0, T]$, and we permute
 110 randomly the timestamps t_q of all temporal edges while keeping the node indices i_q and j_q fixed. We
 111 emphasize that the resulting aggregated structure is the same as in the original data, so that the static RC
 112 is exactly the same in the data and in the null model. Moreover, the activity timeline is also the same:
 113 differences in the cohesion and in the temporal rich club coefficient between the data and the null model
 114 makes it thus possible to distinguish between simultaneity of links due purely to e.g. bursts of activity and
 115 simultaneity due to more meaningful structures.

116 Furthermore, as $M(k, \Delta)$ is defined as a maximum over time, it is also relevant to study the time
 117 evolution of the Δ -cohesion $\varepsilon_{>k}(t, \Delta)$, in order to find the moments of highest simultaneous connectivity
 118 of $S_{>k}$, and to check whether this cohesion is stable or fluctuates strongly (similarly to the fact that single
 119 nodes can have stable or fluctuating high degree²⁷). This quantity can be shown, as in Figure 1d-e, as a
 120 colormap of $\varepsilon_{>k}(t, \Delta)$ vs. t and Δ at fixed k , (or t and k at fixed Δ), or as curves ($\varepsilon_{>k}(t, \Delta)$ vs. t at fixed Δ
 121 and k). This allows for instance to distinguish between stable or recurrent and transient rich club effects:

122 in the former case, $\varepsilon_{>k}(t, \Delta)$ reaches its maximum $M(k, \Delta)$ repeatedly, or remains close to it, while in the
 123 latter, $M(k, \Delta)$ is reached only once or only at specific moments. We can moreover compare $\varepsilon_{>k}(t, \Delta)$
 124 for the data and for the null model, in which the activity timeline and the static rich-club structure are
 125 conserved, to reveal which temporal patterns cannot be simply explained by e.g. periods of higher activity.

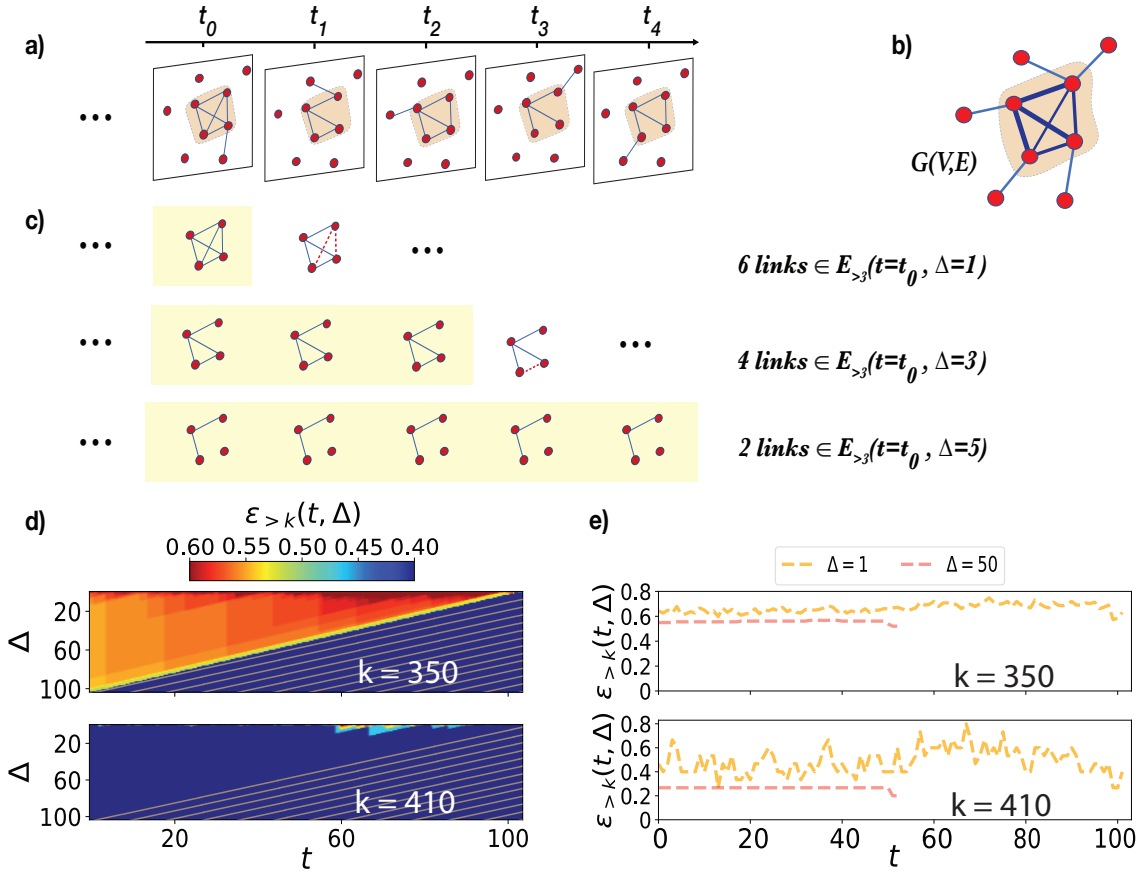


Figure 1. **a)** Schematic representation of a temporal network as a sequence of instantaneous snapshots where nodes are connected by temporal edges. **b)** Time aggregated graph $G(V, E)$, where the weight of an edge corresponds to the number of occurrences of the corresponding temporal edge. The set $S_{>3}$ of nodes of degree larger than 3 in the aggregate graph G and its induced subgraph are highlighted by the shaded area. **c)** Each line shows the edges that form $E_{>3}(t_0, \Delta)$, i.e., the edges joining nodes of $S_{>3}$ that are stable on $[t_0, t_0 + \Delta]$, for several values of Δ , for the toy example of panel a). **d)** Two examples of colormaps of the Δ -cohesion $\varepsilon_{>k}(t, \Delta)$ vs. t and Δ at fixed k , computed for the U.S. Air Transportation Temporal Network, for $k = 350$ and $k = 410$. The characteristic triangular shapes in these colormaps is due to the following property: if an edge (or a set of edges) is stable from a time t to a time $t + \Delta$, it is also stable from $t + 1$ to $t + 1 + (\Delta - 1)$, from $t + 2$ to $t + 2 + \Delta - 2$, etc. Each edge contributing to the density value at coordinates (t, Δ) in the colormap thus also contributes to the value at $(t + n, \Delta - n)$. Note that $\varepsilon_{>k}(t, \Delta)$ gives the density of edges stable on $[t, t + \Delta]$, so is not defined for $t > T - \Delta + 1$. **e)** Examples of time series $\varepsilon_{>k}(t, \Delta)$ vs. t , at fixed k and Δ , for the same data set, i.e., horizontal cuts of the colormaps.

2.2 Static vs. temporal rich clubs

We first apply our measure on a data set describing the U.S. air transportation infrastructure from 2012 to 2020, with temporal resolution of one month, for 105 snapshots (see Methods): in this temporal network, the $N = 1920$ nodes represent airports and a temporal edge in one snapshot represents the existence of a direct connection in the corresponding month. The average number of temporal edges in a snapshot is 6126 and, in the aggregated network, the average degree is 44, with degrees ranging from 1 to 498. We show in the Supplementary Information (SI) the degree distribution of the aggregated network as well as of several snapshots: as discussed in⁴³, these distributions are broad and stable across months and years, despite some fluctuations in the instantaneous degrees of single nodes.

Figure 2.a shows the $k - \Delta$ diagram of the temporal rich club coefficient $M(k, \Delta)$ as a color plot (the size of $S_{>k}$ being shown on top). At fixed k , $M(k, \Delta)$ decreases as Δ increases (by definition, as a larger Δ is a stronger requirement in terms of stability of temporal edges). At fixed Δ , $M(k, \Delta)$ is small for small and intermediate k , and decreases rapidly as Δ increases: many small airports have fluctuating activity, sometimes seasonal, so that many temporal edges involving these airports are not very stable⁴³, leading to a small cohesion at the global level. The maximal cohesion however increases with k : airports with more connections tend also to be more interconnected and with increasingly stable connections (as found also in⁴³). $M(k, \Delta)$ reaches very large values around $k \sim 315$, even at large Δ , indicating a stable and very cohesive structure. In fact, most of the 31 airports in $S_{>315}$ are hubs of the U.S. air transportation system, which are largely interconnected with very stable (and simultaneous) connections. We note that: (i) the cohesion reaches 1 for $\Delta = 1$, meaning that there exists at least one month in which these nodes are all simultaneously interconnected, however (ii) the cohesion remains lower than 1 for $\Delta > 1$, meaning that not all these connections are stable. For higher values of k , $M(k, \Delta)$ decreases again, especially at large Δ , with a final increase close to the maximum possible value of k (such that $|S_{>k}| \geq 2$). This pattern indicates that, when restricting to $k > 380 - 390$, the interconnections of the nodes of $S_{>k}$ become actually less simultaneous and stable than in $S_{>315}$: this means that some airports with degree larger than 380 - 390 have actually less stable connections than others with degree $315 < k < 380$, i.e., that some of the airports with very large aggregated degree have fluctuating connections, even if their instantaneous degree remain stable, see Figure 2d. This is also clear from the cohesion shown in Figure 1.d-e for $k = 350$ and $k = 410$, with large and stable values for $k = 350$ at any Δ , but smaller values for $k = 410$ and large fluctuations

155 at small Δ . While the static rich-club analysis shown in Figure 2c does not reveal any such pattern, the
156 analysis of the cohesion shows that the nodes with very high degree have a counter-intuitive behaviour
157 with less stable connections than nodes with slightly less high degree.

158 We further investigate this point in Figure 2.b,d: Figure 2.b shows the 20 airports with largest
159 aggregated degree, i.e., number of distinct other airports with which they share a direct connection (degree
160 values ranging from 350 to 498). We highlight in red the airports that are as well among the 20 nodes with
161 largest aggregated strength ($s > 10,000$), and in light blue the others. While the red nodes are typically
162 well-known hubs, we find among the nodes in light blue airports such as Burbank-Hollywood (BUR),
163 Teterboro Airport (TEB) and Westchester County Airport (HPN). It turns out these airports serve as
164 reliever airports for hubs such as LAX (Los Angeles) and JFK (New York), respectively: they are therefore
165 extremely well connected in the aggregated network but have fluctuating connections, depending on the
166 needs of the neighbouring hubs. Figure 2.d highlights the differences between the two types of nodes,
167 i.e. the "real" hubs and the reliever airports. On the one hand, both hubs and relievers have rather stable
168 values of their instantaneous degree $k(t)$. The relievers cannot be simply identified as unstable hubs²⁷, i.e.
169 by a strongly fluctuating instantaneous degree. On the other hand, the bottom panel displays the Jaccard
170 index between the connections of O'Hare International Airport (ORD) and Westchester County Airport
171 (HPN) in successive months. ORD has a very stable neighborhood while HPN (reliever airport for JFK),
172 despite having the largest aggregated degree value, undergoes changes of up to 80% of its neighborhood
173 from a month to the next: as also shown in the SI, the neighborhoods of reliever airports, and not of hubs,
174 change between successive snapshots: it is thus the dynamics of their neighborhoods that identifies reliever
175 airports⁴², rather than the evolution of their instantaneous degree.

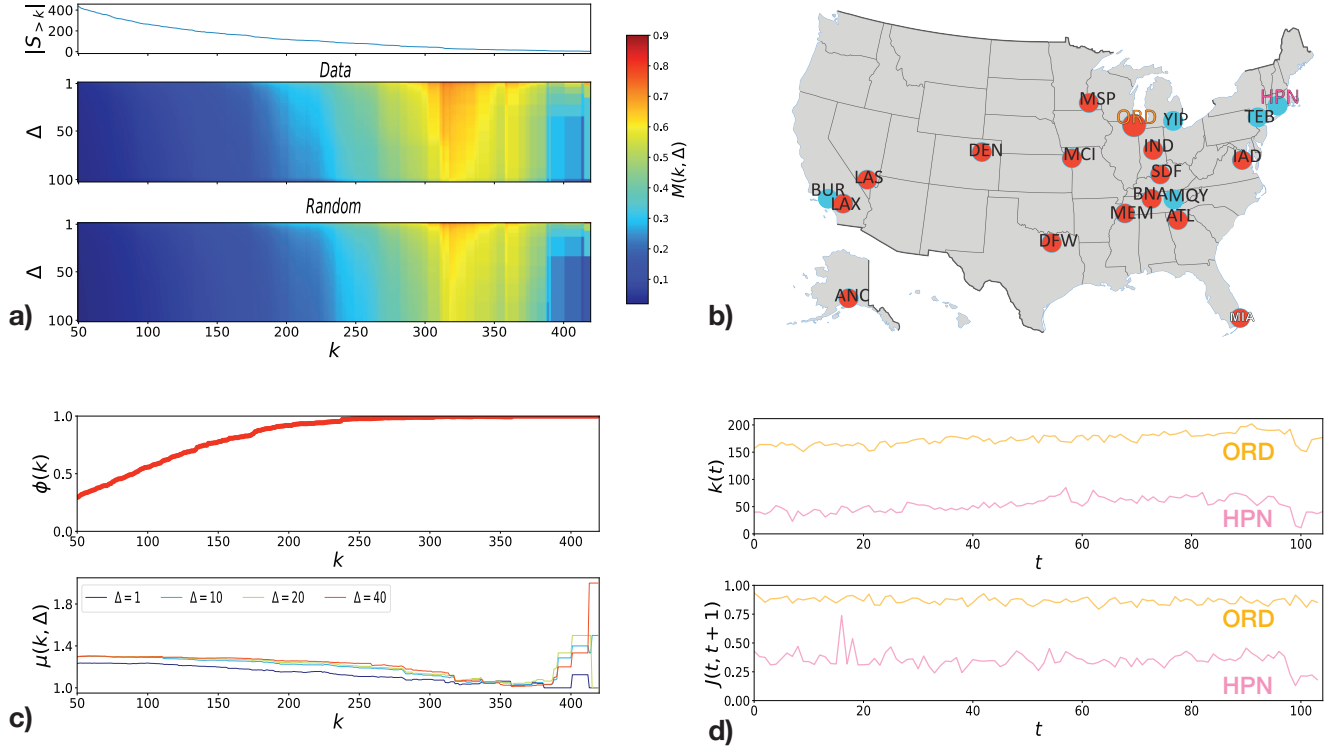


Figure 2. U.S. air transportation temporal network. **a)** (top) Size $N_{>k} = |S_{>k}|$ of the sub-network of nodes of aggregate degree larger than k as a function of k ; (middle) temporal rich club coefficient $M(k, \Delta)$ as a color plot as a function of k and Δ , for the U.S. air transportation temporal network; (bottom) $M_{ran}(k, \Delta)$ obtained for a randomized version of the temporal network that preserves the activity timeline and the structure of the aggregated network. **b)** Geographic locations of the 20 airports with largest aggregate degree ($S_{>350}$); airports that are also in the group of 20 nodes with highest strength ($s > 10,000$, i.e., at least about 100 different connections each month on average) in the aggregated network are depicted in red, whereas the light blue nodes have low strength. **c)** (top) Static rich club coefficient $\phi(k)$ of the aggregated graph, as a function of the aggregate degree k ; (bottom) ratio $\mu(k, \Delta)$ between $M(k, \Delta)$ and $M_{ran}(k, \Delta)$ as a function of k for specific values of Δ . $\mu(k, \Delta) > 1$ indicates that a temporal rich club ordering is present, i.e., that the interactions within $S_{>k}$ are more simultaneous than expected by chance. **d)** Instantaneous degree and Jaccard index of the neighborhood of a node between times t and $t + 1$ (bottom) as a function of time, computed for O'Hare International Airport (ORD), and Westchester County Aiport (HPN): both airports are in the top 20 nodes for aggregate degree, yet ORD has also a stable neighborhood while the one of HPN fluctuates more.

Figure 2.a (bottom) displays the maximal cohesion $M_{ran}(k, \Delta)$ for the randomized version of the data. $M_{ran}(k, \Delta)$ shows similar patterns but smaller values than $M(k, \Delta)$ for all (k, Δ) , showing that a temporal rich club ordering is present: for any $S_{>k}$, the interactions tend to be more simultaneously cohesive than expected by chance. This is the case even at very large k : even when the reliever airports lead to a smaller $M(k, \Delta)$, its value is still larger than by chance.

Differences with chance expectations are further investigated in Figure 2.c, which also shows for reference the static rich club coefficient $\phi(k)$. $\phi(k)$ increases monotonically and saturates at 1 for k larger than ~ 300 , with thus a simpler pattern than $M(k, \Delta)$. The ratio $\mu(k, \Delta)$ vs. k for various Δ exhibits on the other hand an interesting behavior: $\mu(k, \Delta)$ is above 1 and almost constant over a large range of k values, and decreases for $320 \lesssim k \lesssim 380$: in this range of k values, $S_{>k}$ is a mix of hubs and reliever airports, with both very stable connections and others much less stable. The randomization by time stamp reshuffling does not perturb the most stable connections, so that M and M_{ran} are closer. Finally for the largest aggregated degree values, $\mu(k, \Delta)$ reaches again very large values, especially for large Δ : many of the remaining connections are to reliever airports (more than 50% of edges between the nodes of $S_{>k}$ for $k > 350$), and, even if these connections are not necessarily very stable nor simultaneous, they are more so than by chance.

We also show in the SI the analysis of the data set if we merge each reliever we have identified with its corresponding hub: as could be expected from the previous discussion, the temporal rich club coefficient is then simply an increasing function of k at fixed Δ , with $M(k, \Delta)$ close to 1 for all $k > 310$ and all Δ , and the large values of $\mu(k, \Delta)$ at large k are suppressed. The patterns of Figure 2 are thus due to the co-existence of hubs and relievers, whose different nature could not simply be inferred from the static rich club coefficient nor by the fluctuation of their instantaneous degrees. We note indeed that the static rich clubs of the two cases (with or without merging of hubs and relievers) are very similar (see SI); however the temporal patterns are very different, especially for the very high degrees: when hubs and relievers are merged, $\varepsilon_{>k}(t, \Delta)$ remains close to 1 for all $k > 310$ and all Δ , indicating an extremely stable densely connected structure present at all times; in the original data, $\varepsilon_{>k}(t, \Delta)$ still does not depend much on time for $310 \lesssim k \lesssim 380$ but takes lower values (hence the structure is less densely connected), and for $k = 410$ it is possible to identify the coexistence between (i) a very stable structure with density ~ 0.3 (ii) links that allow to reach a larger cohesion but only at specific moments in time and for limited durations (smaller Δ).

Overall, the analysis of the US air transportation network under the lens of the temporal rich club has thus shed light on the different roles of well-connected nodes, highlights how temporal and static rich clubs can co-exist albeit with different patterns, and how a given static rich club pattern can correspond to very different temporal rich club dynamics.

2.3 Temporal rich club and spreading processes

The second dataset we consider is a temporal network of face-to-face interactions between 232 students and 10 teachers of a primary school in France¹²: the temporal edges between two nodes at a specific time stamp correspond to the detection by wearable sensors of a face-to-face interaction between the two corresponding individuals at that time, as in similar data sets studied in previous works on temporal networks^{11,27,44,45} (see Methods). The original time resolution of the data set is 20s for two schooldays, and, in order to smoothen the short time noisy dynamics, we perform a temporal coarse-graining on successive time-windows of 5 minutes. We consider in the main text the first school day only, i.e., a temporal network of $N = 242$ nodes and duration $T = 103$ time stamps (each representing a 5-minutes time window). The maximal degree in the aggregated network is $k_{max} = 98$ (see SI for the degree distribution of the aggregated network). Results for the whole 2-days data set and for a finer temporal resolution are shown in the SI. We also show and discuss in the SI the analysis of other data sets describing face-to-face interactions in other contexts.

Figure 3.a displays the $k - \Delta$ diagrams of $M(k, \Delta)$ for the original temporal network (middle) and its randomized version ($M_{ran}(k, \Delta)$, bottom), with the size of $S_{>k}$ (top panel), as for Fig. 2a. At fixed Δ , $M(k, \Delta)$ tends to increase with k ; moreover, $M(k, \Delta)$ decreases more slowly with Δ when k increases: nodes with higher degree in the aggregated network tend to be more tightly interconnected, and in a more stable way. This gives additional insights into the social dynamics of the school, by showing that the static rich club is not only due to contacts occurring at unrelated times, but that a cohesive structure between the high degree nodes actually took place in a simultaneous way. For instance, the 7 nodes of $S_{>87}$ reach a maximal cohesion $M(k, \Delta) \approx 0.28$ at $\Delta = 1$ and have some long lasting stable contacts ($M(k, \Delta) \gtrsim 0.09$ up to $\Delta = 25$). We have verified that the students of $S_{>87}$ actually belong to different school classes: the static rich club could thus a priori be due to random, fleeting contacts occurring at unrelated times between them, but the value reached by $M(k, \Delta)$ shows that a part of the structure found statically is indeed found

as simultaneous links at least once. Note however that the instantaneous cohesion remains lower than the static rich club coefficient: only a fraction of the links present in the aggregated network are present simultaneously at any instant ($\phi(k)$ reaches values close to 0.9, while the instantaneous cohesion $M(k, \Delta)$ remains lower than 0.3).

The temporal structures disappear in the randomized version of the temporal network (which has the same static rich-club as the original data), with much lower cohesion values on the whole $k - \Delta$ domain, indicating a temporal rich club ordering in the data i.e., that the cohesion between the large degree nodes cannot be simply explained by the activity timelines. This is confirmed in Figure 3.b, in which we investigate the dynamics of the temporal rich club through the temporal evolution of the cohesion $\varepsilon_{>87}(t, \Delta)$. For the original data, the simultaneous cohesion of these nodes fluctuates strongly at small Δ , is 0 in many snapshots and reaches its maximum in the periods of high overall activity (namely recess and lunch break¹², as seen from the activity timeline of the network), forming a transient but repeated temporal rich club (just as single nodes can also repeatedly have large numbers of neighbours, or small structures -motifs- can also appear repeatedly in some cases²⁸). We also show in the SI that some cohesion between these nodes occurs again in the class breaks of the second day of data, albeit in a less stable way. For large Δ , the rich club is clearly transient, with large cohesion values only during the lunch break (we have verified that these students actually belong to different school classes, which explains why the moments of highest cohesion of this group can only happen during the breaks). In the randomized data instead, these patterns are suppressed. Note that, while the analysis of static RCs on each snapshot could reveal that small cohesive structures between these nodes appear repeatedly, it would not allow to investigate their stability, as the links of these instantaneous rich clubs could differ from one time to the next. We show for instance in the SI the cohesion diagrams as a function of time and degree, for various values of Δ : $\varepsilon_{>k}(t, \Delta = 1)$ reaches values of ≈ 0.25 in several periods, but a same density of 0.25 in successive times could correspond to completely different links. This is actually the case in the reshuffled data (even if the instantaneous rich club connectivity reaches similar values as in the real data in a repeated fashion), as the investigation of $\varepsilon_{>k}(t, \Delta > 1)$ shows: it remains larger than zero for $\Delta \geq 5$ only for the original data and during the lunch break. In other words, patterns of apparent stability seen in instantaneous static rich club values do not correspond necessarily to a real stability of the link structure. Studying the Δ -cohesion with $\Delta > 1$ makes it possible to distinguish between these possibilities: Figure 3.b, shows that the link structure between the large degree nodes is also partially present for large Δ , although with few links for $\Delta > 10$;

it becomes moreover transient, i.e., the cohesive structure between these students occurs only once in a stable manner, namely at lunch. Note also that this transient structure is an indication that the network structure is different during lunch with respect to other periods, as indeed found by other analysis^{41,46}. In the randomized data instead, in which both activity timelines and static RC are conserved, these patterns are suppressed: this highlights once again how the stability and transient or repeated character of the rich club structure could not be deduced from the analysis of the static RC nor of the activity timeline.

Figure 3c shows for reference the static rich club coefficient $\phi(k)$, which increases with k , as with other social networks¹⁷: the children with a larger diversity of contacts (the degree in the aggregated network is the number of distinct other individuals contacted) tend also to be more interconnected. For the temporal rich club coefficient, the ratio $\mu(k, \Delta)$ quantifies moreover the difference in simultaneous interactions with respect to the randomized version: it is higher for larger Δ , as stable simultaneous interactions are disrupted in the null model, remains stable on a broad range of k values, and tends to decrease at larger k . This indicates that the nodes of the temporal network are connected in a much more simultaneous way than expected by chance, especially when considering stable interactions (i.e., temporal edges lasting over many successive snapshots). Once again, this result could not be deduced from the static rich club analysis, even if applied successively to each snapshot.

The temporal network under scrutiny represents interactions among individuals, which can be the support of many processes, and in particular of the spread of information or infectious diseases. It is thus relevant to investigate whether the temporal rich club ordering plays a role in the unfolding of such processes, as with other temporal structures³⁸. We therefore consider the paradigmatic susceptible-infected-susceptible (SIS) and susceptible-infected-recovered (SIR) models of spreading processes. In the SIS case, nodes can be either susceptible (S) or infectious (I): a susceptible can become infectious upon contact with an infectious, with probability λ per time step; infectious individuals recover with probability ν at each time step and become susceptible again. In the SIR case, nodes enter the R compartment upon recovering and cannot be infected again. We quantify the interplay between the temporal network and the spread by the epidemic threshold λ_c at given ν (the epidemic thresholds of the SIS and SIR models have been shown to coincide⁴⁷): it separates a phase at $\lambda < \lambda_c$ in which the epidemic dies out from a phase at $\lambda > \lambda_c$ where it reaches a non-zero fraction of the population. We compute the epidemic threshold, using the method of⁴⁸, in (i) the original data set (λ_c^{data}) and (ii) versions of the data set in which the timestamps of the temporal edges connecting the nodes in $S_{>k}$ are randomized (λ_c^{rand}), thus disrupting

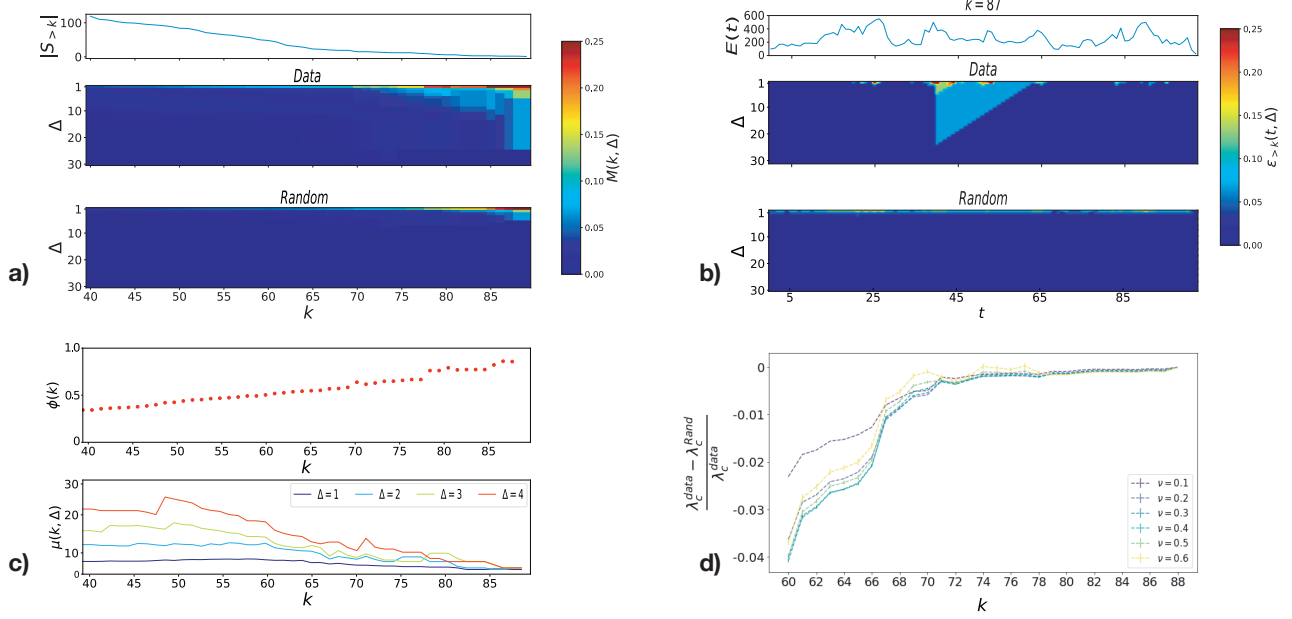


Figure 3. Primary school temporal network. **a)**(top) Size $|S_{>k}|$ of the sub-network of nodes of aggregate degree larger than k as a function of k of the Primary School temporal network; (middle) Maximal cohesion $M(k, \Delta)$ as a function of k and Δ ; (bottom) $M_{ran}(k, \Delta)$ diagram of the randomization preserving aggregate node statistics and overall activity timeline. **b)** (top) Activity timeline of the network, i.e., number of temporal edges at each time step; (middle) Colormap of the cohesion $\epsilon_{>k}(t, \Delta)$ vs. t and Δ ; (bottom) Colormap of the same cohesion for the randomized data. **c)** (top) Static rich club coefficient $\phi(k)$ computed for the aggregated graph as a function of the aggregate degree k ; (bottom) ratio $\mu(k, \Delta)$ between $M(k, \Delta)$, computed for the data, and $M_{ran}(k, \Delta)$, for different values of Δ . **d)** Relative difference between the epidemic threshold λ_c^{data} , computed for the original dataset, and λ_c^{rand} , computed after the randomization of the interactions between the nodes of $S_{>k}$ (see Methods).

their simultaneity (see Methods). Figure 3.d displays the relative difference between the two obtained values as a function of k . This difference takes higher absolute values for lower values of k , which can be expected as the randomization affects then a larger number of temporal edges; most importantly, λ_c^{data} is systematically lower than λ_c^{rand} : this indicates that the spreading process is favoured by the temporal rich club of the data, i.e., by the stronger simultaneity of connections than in the randomized versions³³. The effect is also larger for larger ν , i.e., for faster processes. The fact that hubs in an aggregated network might in fact have fluctuating degrees^{27,33}, as well as the simultaneity of other structures³⁸, have been shown to impact spreading processes. The temporal rich club analysis thus reveals cohesive simultaneous structures of prominent nodes that affect spreading dynamics.

2.4 State-specific temporal rich clubs: similar static but distinct temporal patterns

We finally investigate the temporal rich club patterns of a network of biological relevance, namely the time-resolved functional connectivity of $N = 67$ neurons in the entorhinal cortex and hippocampus of an anesthetized rat. The nodes represent single neurons and the temporal edges correspond to a significant mutual information between the firing patterns of pairs of neurons in a sliding window of 10 seconds^{29,49}, as shown in Figure 4a. Successive time windows are shifted of 1 second: this is the temporal resolution of the network, which lasts 2284 seconds. We also consider in the SI a similar data set describing the temporal functional connectivity of neurons in an epileptic, anesthetized rat⁵⁰, and highlight similarities and differences between both cases.

We first note that the aggregated network is very dense: the average degree is $\langle k \rangle = 54$ (whereas the minimal value of k is $k_{min} = 14$) and the maximal degree is equal to $N - 1 = 66$ (see SI for the aggregated network degree distribution). In such a dense network, the static rich club ordering cannot be assessed as randomization of the links is impossible to achieve in practice. Taking into account temporality reveals a more interesting picture. Figure 4.b shows that the temporal rich club coefficient $M(k, \Delta)$ increases with k for each value of Δ , and that groups of nodes with increasing aggregated degree are simultaneously interconnected for increasing durations. The group of 8 neurons with largest degree (which are each connected at least once over the temporal network duration to each of the other nodes) are in particular very strongly interconnected in a simultaneous and stable way, with $M(k, \Delta) \geq 0.5$ up to $\Delta = 150$ (reaching even $M(k, \Delta) = 1$, i.e., the fully connected link structure of these 8 neurons seen in the static aggregated graph does occur at some time in a simultaneous way).

$M_{ran}(k, \Delta)$ takes much smaller values

for most values of k and Δ , see SI, indicating the existence of a temporal rich club ordering in this data set: even if the neurons with largest degree share some simultaneous connections also in the null model, the corresponding structure is never simultaneously fully connected, and is not stable.

While this analysis corresponds to the TRC computed over the whole temporal network, it is worth investigating in more details the dynamical patterns of the cohesion. Indeed, the temporal network of functional connectivity actually goes through several "states"²⁹. These states are identified by the method pioneered in²⁸ and recently developed in⁴¹ (Figure 4c): one computes the network similarity matrix, in

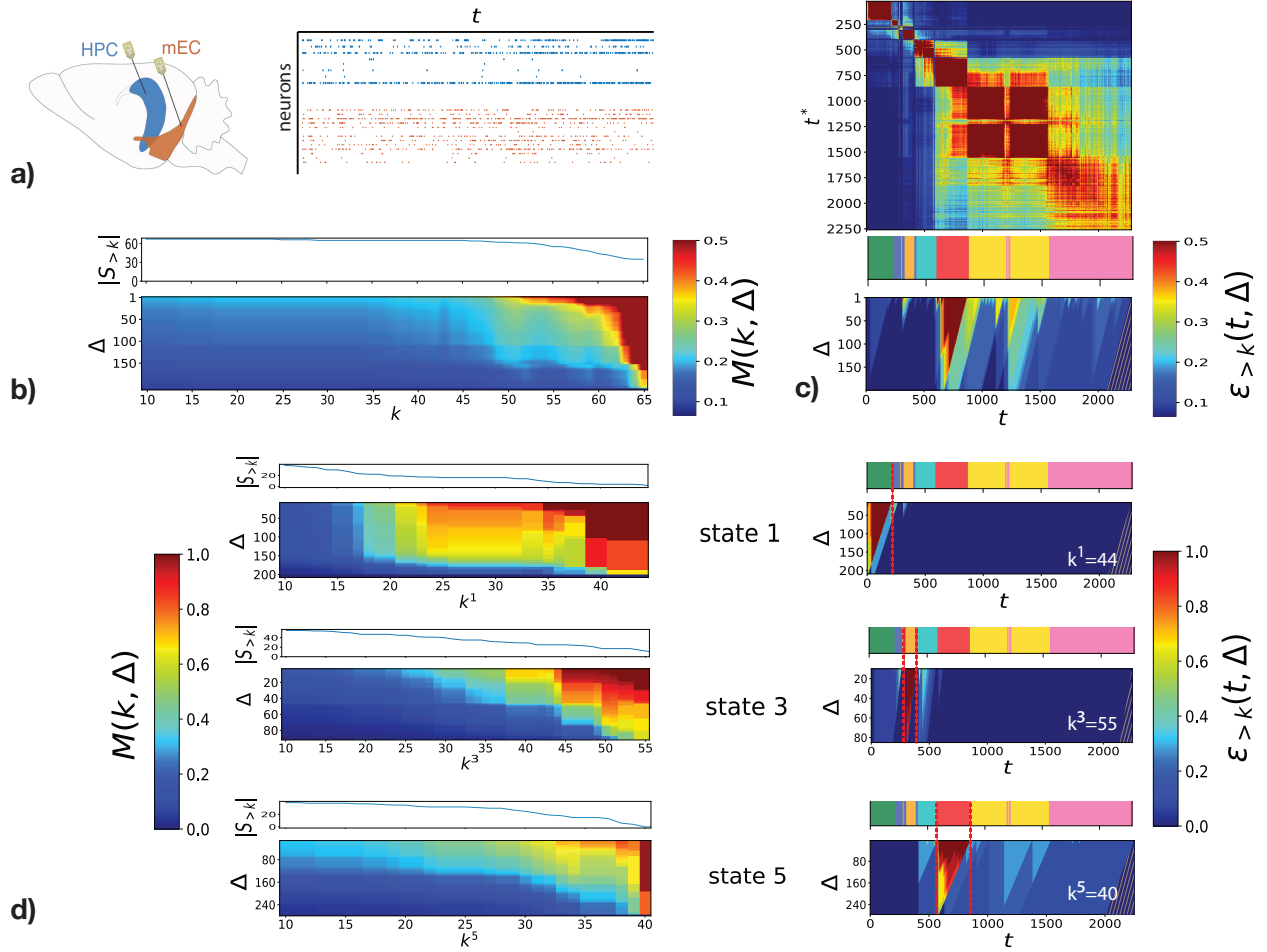


Figure 4. Temporal network of information sharing neurons. **a)** Sketch of the brain areas (enthorinal cortex, mEC, and hippocampus, HPC) and electrodes recording the firing signal of single neurons (as shown in the right part of the panel). **b)** (top) Size $|S_{>k}|$ of the sub-network of nodes of aggregate degree larger than k as a function of k ; (bottom) Maximal cohesion $M(k, \Delta)$ as a function of k and Δ . **c)** Temporal network similarity matrix: the (t, t^*) matrix entry is given by the similarity between the instantaneous snapshots of the network at times t and t^* . The red blocks around the diagonal indicate periods in which the network remains similar to itself, i.e., "states" of the network^{29,33}: we show below the matrix the timeline of these states as a colored barcode (each color represents a different state), as extracted by clustering of the similarity matrix in²⁹. In addition, we show below this timeline the colormap of the cohesion $\varepsilon_{>65}(t, \Delta)$ of the $N_{>65} = 8$ nodes of aggregate degree larger than $k = 65$ as a function of t and Δ , showing patterns at different times and that the temporal rich club is transient and mostly concentrated at the times corresponding to a specific state. **d)** For three different states (states 1, 3 and 5), we show in the left column the size $|S_{>k}|$ of the sub-network of nodes of aggregate degree larger than k and the maximal cohesion $M(k, \Delta)$, and in the right column the cohesion $\varepsilon_{>k}(t, \Delta)$ of the nodes with highest degree in the aggregate graphs of the corresponding states (respective largest degree values: 45, 56 and 41); the sets have sizes $|S_{>44}^1| = 5$, $|S_{>55}^3| = 7$ and $|S_{>40}^5| = 7$; $S_{>44}^1$ has 1 node in common with $S_{>55}^3$, and $S_{>40}^5$ has no node in common with $S_{>44}^1$ nor with $S_{>55}^3$.

330 which each element (t, t^*) gives the similarity between the snapshots of the network at times t and t^* ;
 331 the hierarchical clustering of this matrix makes it possible to identify periods of stability of the network
 332 ("states") as periods of large similarity values. This is the case in various types of data^{28,41,51} and in
 333 particular in the present data set²⁹, as shown in Figure 4.c (red blocks along the diagonal, with underneath
 334 the timeline of successive states). The figure also shows the colormap of the cohesion $\varepsilon_{>65}(t, \Delta)$ of the
 335 nodes with highest degree in the network aggregated on the whole recording: the cohesion among these
 336 nodes changes strongly from one state to another, and actually reaches very large values only during one
 337 specific state. Note that, even if the TRC analysis by itself does not allow to uncover and define precisely
 338 the network states, the cohesion diagram of Figure 4.c in itself is a strong indication that (i) there exists at
 339 least one period of stability in the network, in which the static RC nodes are very cohesive (ii) there are
 340 specific periods of time with distinct dynamics, and thus it is relevant to look for network states. Such
 341 insights could not be obtained by investigating only the activity timeline and the static rich club, nor
 342 the instantaneous rich club on each time stamp. This is made clear in the SI by comparing the network
 343 similarity matrix and the $\varepsilon_{>k}(t, \Delta)$ colorplots of the real data and of the null model with the same timeline
 344 and static rich club as the data: indeed, (i) the states are scrambled in the null model; (ii) $\varepsilon_{>k}(t, \Delta = 1)$,
 345 giving the instantaneous rich club density, reaches high values during several periods for both data and
 346 null model, indicating the existence of simultaneous connections among the high degree nodes in both
 347 cases; as soon as Δ increases however, this cohesion disappears for the null model, showing that no stable
 348 structure is in place, while it remains high for large values of Δ at specific periods in the real data.

349 We thus investigate separately these different states, computing an aggregated network G^s for
 350 each state s by aggregating the temporal edges in the snapshots belonging to s , and defining $S_{>k}^s$ as the set
 351 of nodes with degree larger than k in G^s : nodes are not similarly active in each state and have thus different
 352 degrees in the different G^s . This leads us to measure the state-specific temporal rich club coefficients
 353 $M^s(k, \Delta)$. Figure 4.d shows that the corresponding $k - \Delta$ diagrams for states 1, 3 and 5 have in each case
 354 more stable simultaneously interconnected sets of nodes as k increases, and a temporal rich club ordering
 355 (we show in the SI that the randomized data sets yield much lower values of M). The SI shows also that
 356 the static rich club patterns of the aggregated networks of these three states are very similar. The sizes
 357 of the sets of nodes with largest degree are also comparable in the three states ($|S_{>44}^1| = 5$, $|S_{>55}^3| = 7$,
 358 $|S_{>40}^5| = 6$). However, the nodes belonging to these three sets are mostly different: of the nodes in $S_{>44}^1$
 359 only one is also in $S_{>55}^3$, and $S_{>40}^5$ has an empty intersection with the other sets. Moreover, the cohesion

colormaps of these sets of nodes, shown in Fig. 4.d and in the SI (with zooms on each state), show that (i) their instantaneous cohesion is maximal (reaching even 1) precisely in the time stamps of the corresponding state (ii) different dynamics are observed despite the similarity in their state-wise static rich clubs: for states 1 and 3, we observe a maximal cohesion for almost all the state duration; for state 5 instead, the maximal cohesion is reached repeatedly but does not last the whole state.

Finally, we highlight in the epileptic brain data set studied in the SI how the cohesion diagram indicates in that case a state with a cohesive rich club, but that the cohesion patterns are less stable than in the non-epileptic case (with cohesive structures lasting much less than the state duration), and how this hint is confirmed by the analysis of the cosine similarity matrix. This is coherent with the results of⁵⁰, according to which the functional connectivity is more disordered in the epileptic brain.

Overall, the analysis of this temporal network highlights how a temporal rich club phenomenon can be present even when a static rich club ordering cannot be identified. Moreover, it shows that distinct temporal rich clubs can be found when a temporal network goes through different states, with similar state-wise static rich-club patterns but different temporal stability patterns. In fact, the TRC analysis can even give hints about the existence of states and their internal dynamics. Further investigation of the mutual relations of the state-wise temporal rich clubs could help shed light on the function of the different states of the system²⁹. In particular, while the core-periphery structure highlighted in²⁹ does not reveal whether the core neurons are interconnected in a stable way, the TRC captures the existence of a subset of neurons with enhanced internal integration not just instantaneously but lasting for a finite time. It might thus provide a translation into a temporal network language of what systems neuroscientists have been calling a cell assembly, as an entity implementing a window for distributed information integration^{52–54}. Different states might in this perspective correspond to the recruitment of different cell assemblies performing different computations.

3 Discussion

An increasing number of studies^{24,26,28,55} have shown how the analysis of temporal networks necessitates specific tools, as the study of static aggregated networks hides e.g. the fact that nodes with large aggregated degree can have a strongly varying connectivity²⁷ or neighborhood⁴²: for instance, the repetition of

simultaneous or successive subgraphs forming temporal motifs^{28,34–36,56} or the emergence of stable strongly connected subgraphs³⁷ cannot be guessed from a static picture. We have defined here a novel concept to investigate temporal networks and quantify the patterns of simultaneous interconnectedness of nodes, namely the Temporal Rich Club (TRC). We have defined the temporal rich club coefficient as the maximal value of the density of links stable during at least a duration Δ between nodes having aggregated degree at least k . We emphasize that the properties of this density cannot be simply reduced to the stable or varying degree of the hubs nor to the existence of subgraphs, although these concepts are naturally interdependent: a stable hub might have only low degree neighbours (i.e., not contributing to a rich club), or have low loyalty⁴², i.e., different neighbours from one time to the next; conversely, a hub might have mostly fluctuating links, i.e., be an unstable hub²⁷, but maintain some stable connections to other hubs and hence contribute to a temporal rich club. We compare the values of the TRC coefficient obtained on an empirical data set to those reached in a randomized version of the data, in order to measure whether the simultaneity and stability of the connections of groups of nodes is higher than expected: a temporal rich club ordering corresponds to more simultaneous cohesion than expected by chance. We note here a delicate point: many randomization procedures are possible for a temporal network⁴⁰. However, to focus on the simultaneity of connections, it is sensible to consider only reshuffling procedures that maintain the network activity timeline and the aggregated properties of the nodes and links, i.e, to simply reshuffle the timestamps of all temporal edges.

In general, different patterns can be observed in terms of temporal rich clubs, even at given static rich club: the links forming a rich club of the static network could correspond to interactions occurring at different times; vice-versa, interactions could be more simultaneous than expected by chance, with a temporal rich club ordering, without a rich club ordering. In the US air transportation case (Figure 2), the static rich club coefficient increases monotonically with k , but the existence of reliever hubs leads to more fluctuating links around large degree nodes, and thus a non-monotonic behaviour of $M(k, \Delta)$ with k . By comparing the original data and a network with merged hubs and reliever airports, we showed how the static rich club patterns are not altered, while the temporal rich club patterns are strongly modified. In the school contact network instead, both static and temporal coefficients show an increasing trend with k (Figure 3). In the other data sets of face-to-face interactions analyzed in the SI, we exhibit on the one hand a similar case with both static and temporal rich clubs, and on the other hand a case where a static rich club does not correspond to any temporally simultaneous structure. In the third data set explored, the static

rich club connectivity is equal to 1 at intermediate and large k , so that the static rich club ordering concept is irrelevant in practice (the links cannot be reshuffled so the null model cannot be defined). Taking into account temporality reveals a more interesting picture and a temporal rich club ordering (Figure 4). The evolution of the instantaneous cohesion reveals an additional diversity of patterns, as the temporal rich club can be present in a rather stable way (Figure 1d), or concentrated around specific periods (Figure 3b, Figure 4c). The temporal patterns of the cohesion can even hint at the presence of different temporal network states stability periods or states (Figure 4c), and highlight different temporal rich-club patterns within these states despite similar state-wise static rich-club patterns. The comparison of the cohesion patterns between temporal networks of different brains (e.g. epileptic vs. non-epileptic, see SI) also indicates differences in their states' internal dynamics.

A limit of our analysis comes from the fact that we have considered the degree of nodes in the aggregate network as the reference for centrality in the aggregate network. A natural extension would be to consider instead the strength of the nodes in the aggregate network, i.e., the number of temporal edges to which they have participated during the span of the temporal network: in this case, the focus would be to investigate the simultaneity of the connections within the set $S_{>s}$ of nodes having participated in more than s temporal edges. As strength and degree are generally correlated, the results are expected to be similar, but some significant and interesting differences might emerge, as in the example of the air transportation temporal network where the reliever airports have a very high degree but relatively low strength.

Overall, the temporal rich club perspective provides a new tool to study temporal networks and in particular to unveil the relevance of simultaneous interactions of increasingly connected nodes in processes unfolding on top of the temporal network: we have shown for instance that a temporal rich club pattern favours spreading dynamics, similarly to other static or temporal cohesive structures^{15,33,38}, suggesting to add such new measure to the repertoire of methods to study contagion processes in networks, and that models of temporal networks should take such structuration into account^{57,58}. Moreover, we have shown how distinct temporal rich club patterns can be found when a temporal network evolves through different states, and provide thus an additional way to characterize such states and their internal dynamics and, possibly, investigate their function. For instance, key processes in neural information processing, such as synaptic plasticity, are critically affected by the timing of neuronal interactions⁵⁹ and different temporal rich clubs in different states may thus enable flexible computations within a same circuit⁴⁹. TRC

might even provide a connection to so-called cell assemblies^{52–54}, with different cell assemblies being recruited in different states. To form a cell assembly, many neurons must remain strongly functionally connected for a certain finite time, in order for the assembly to be detected by some reader system⁶⁰. This type of firing coordination –which is both distributed in space and lasting in time– is captured only partially by commonly used methods, which seek either for instantaneous synchrony or for sequential firing^{61,62}. However, the temporal rich club notion here introduced precisely captures both criteria needed to qualify a set of co-firing neurons as an assembly. For this reason, we expect the temporal rich club to join the toolbox of network neuroscience for the investigation of dynamic functional connectivity patterns. In conclusion, our work provides a new procedure to detect relevant temporal and structural patterns in a temporal network, enabling a new quantitative perspective on the temporal patterns of data sets coming from very different fields, from highlighting the role of simultaneous connections between central nodes in spreading on a temporal network of social interactions to that of hubs in air transportation infrastructures or in neuronal assemblies.

4 Methods

4.1 Data

We consider three publicly available data sets. We have moreover gathered them at

<https://github.com/nicolaPedre/Temporal-Rich-Club/>

Air Transportation Network. This data set represents the connections between US airports, with temporal resolution of one month, from January 2012 to September 2020, for a total of 105 time stamps. The $N = 1920$ nodes of the temporal network represent the airports, and in each monthly snapshot a temporal edge is drawn between two nodes if there was at least one direct flight between the corresponding airports during that month. The degree of a node in the aggregated network is thus the number of other airports to which it has been connected directly once, and its strength is its total number of temporal edges. We show in the SI the degree distribution of the aggregated network and of some monthly snapshots, as well as some additional temporal properties of the data.

The data is publicly available on the website of the Bureau of Transportation Statistics

473 (<https://www.transtats.bts.gov/>, "Air Carrier Statistics (From 41 Traffic) - U.S. Carriers" data base).

474 **Face to face interactions.** This data set describes the face-to-face close proximity contacts between
475 232 children and 10 teachers in a Primary School of Lyon, France, during two days in 2009, as collected
476 by the SocioPatterns collaboration using wearable devices. The original data is publicly available from the
477 SocioPatterns website (<http://www.sociopatterns.org/datasets/primary-school-temporal-network-data/>).
478 The original data is a temporal network with temporal resolution of 20s, where the nodes represent
479 the individuals and each temporal edge corresponds to the detection of a face-to-face contact between
480 them¹². Here, we perform a temporal coarse-graining on successive time-windows of 5 minutes to remove
481 short-time noise. We show in the SI the degree distribution of the aggregated network and some timelines
482 of instantaneous degree.

483 The results in the main text correspond to the first day of data while the analysis performed
484 on the whole data set can be found in the SI, as well as the results obtained with a coarse-graining on
485 time-windows of 1 minute.

486 **Information sharing neurons.** This data set describes the functional connectivity between neurons in
487 the hippocampus and medial entorhinal cortex of an anesthetized rat. The data was first presented in⁴⁹ and
488 further analysed in²⁹. The network analysed here is made of $N = 67$ nodes. Each temporal edge represents
489 a “functional connection”, i.e. the existence of a significant mutual information between the firing patterns
490 of the corresponding pair of neurons computed in a sliding window of 10 seconds. Overlapping sliding
491 windows are considered, each being shifted of 1 second with respect to the previous one. The duration
492 of the temporal network is $T = 2284$ seconds. More details about the computation of time-resolved
493 functional connectivity can be found in the original studies^{29,49}.

494 We show in the SI the degree distribution of the aggregated network over the whole temporal
495 network and over specific states.

496 4.2 Temporal network randomization

497 We consider a temporal network in discrete time $TN(V, \Gamma, T)$ as a set of nodes $V = \{i = 1, 2, 3 \dots N\}$
498 and a set of temporal edges $\Gamma = \{\gamma_1, \gamma_2, \dots \gamma_T\}$ where each temporal edge $\gamma_q = (i_q, j_q, t_q)$ represents an

Table 1. Some properties of the data sets

Data	N	k_{min}	k_{max}	$\langle k \rangle$	# temporal edges	time resolution, T
U.S. Airways	1,920	1	498	44	1,286,616	$t = 1$ month, $T = 105$
Primary School	242	1	98	49	53,056	$t = 5$ minutes, $T = 103$
Info. sharing network	67	14	66	53	511,174	$t = 1$ s, $T = 2,284$

interaction between nodes i_q and j_q at time $t_q \in [0, T]$. An event or contact (i, j, t, τ) is moreover defined as an uninterrupted succession of temporal edges between nodes i and j starting at t and lasting τ time steps, i.e., a series of temporal edges $(i, j, t), (i, j, t+1), \dots, (i, j, t+\tau-1)$. Furthermore, the "activity" of the temporal network at time t is simply the number of temporal edges at t . The aggregated network $G = (V, E)$ is obtained by drawing an edge between all pairs of nodes that have interacted at least once during $[0, T]$.

A wide range of randomization procedures (null models) exist for temporal networks⁴⁰. Here, our focus is on the simultaneity and stability of interactions, which define the existence of temporal rich club phenomena. As simultaneous interactions can occur simply by chance in periods of larger activity, we will consider randomization procedures that preserve the temporal activity timeline, i.e., the number of temporal edges at each time step. Moreover, in order to investigate the role of temporality, we need to consider a procedure that keeps the whole structure of the aggregated network G , i.e., the number of temporal edges among each pair of nodes. We thus consider the timestamps shuffling null model: this reshuffling procedure, denoted $P[w, t]$ in⁴⁰, randomly permutes the timestamps t_q of all temporal edges while keeping the nodes indices i_q and j_q fixed.

In the present work, we consider moreover two types of data randomization: either the randomization of the whole temporal network, or a randomization involving only the subgraph induced by the set $S_{>k}$ of nodes of degree larger than k in the aggregate graph, while keeping all the other temporal edges fixed. The former case allows us to compare the temporal rich club coefficient $M(k, \Delta)$ of the data with the values obtained for a null model, and thus to detect whether a temporal rich club ordering is present. The latter case is used in Section 2.3 to compare the epidemic threshold in the original data and in a partially reshuffled data set where the simultaneity of the connections between the nodes of degree larger than k (i.e., in $S_{>k}$) is disrupted while the rest of the connections are unchanged.

For each data set, we compute 100 realisations of the randomized data set and compute the

523 average M_{ran} of the temporal rich club coefficient over these realisations.

524 **Data availability statement**

525 All the data used in this work are available at

526 <https://github.com/nicolaPedre/Temporal-Rich-Club/>

527 **Code availability statement**

528 The analysis presented here were performed in python. Example notebooks are available at

529 <https://github.com/nicolaPedre/Temporal-Rich-Club/>

530 The randomized reference models were obtained thanks to the publicly available notebooks by
531 the authors of⁴⁰, namely at

532 <https://github.com/mgenois/RandTempNet>

533 **Funding**

534 N.P. has received funding from the European Union’s Horizon 2020 research and innovation programme
535 under the Marie Skłodowska-Curie grant agreement No. 713750. Also, the project has been carried out
536 with the financial support of the Regional Council of Provence- Alpes-Côte d’Azur and with the financial
537 support of the A*MIDEX (ANR-11-IDEX-0001-02), funded by the Investissements d’Avenir project
538 funded by the French Government, managed by the French National Research Agency (ANR).

539 D.B. is supported by the European Union Innovative Training Network “i- CONN” (H2020 ITN 859937)

540 A.B. is partially supported by the Agence Nationale de la Recherche (ANR) project DATAREDUX
541 (ANR-19-CE46-0008).

542 **Author contributions statement**

543 N.P., D.B. and A.B. designed the study and the experiment. N.P. developed the numerical tools, and
544 produced the figures. N.P., D.B. and A.B. analyzed the data and results and wrote and reviewed the
545 manuscript.

546 **Competing interests**

547 The authors declare no competing interests

548 **References**

- 549 **1.** Albert, R. & Barabási, A.-L. Statistical mechanics of complex networks. Rev. Mod. Phys. **74**, 47–97,
550 DOI: [10.1103/RevModPhys.74.47](https://doi.org/10.1103/RevModPhys.74.47) (2002).
- 551 **2.** Dorogovtsev, S. N. & Mendes, J. F. F. Evolution of networks: From biological nets to the Internet and WWW
552 (Oxford University Press, Oxford, 2003).
- 553 **3.** Barrat, A., Barthélemy, M. & Vespignani, A. Dynamical processes on complex networks (Cambridge
554 university press, 2008).
- 555 **4.** Flake, G., Lawrence, S., Giles, C. & Coetzee, F. Self-organization and identification of web commu-
556 nities. Computer **35**, 66–70, DOI: [10.1109/2.989932](https://doi.org/10.1109/2.989932) (2002).
- 557 **5.** Barrat, A., Barthélemy, M., Pastor-Satorras, R. & Vespignani, A. The architecture of complex
558 weighted networks. Proc. Natl. Acad. Sci. **101**, 3747–3752, DOI: [10.1073/pnas.0400087101](https://doi.org/10.1073/pnas.0400087101) (2004).
559 <https://www.pnas.org/content/101/11/3747.full.pdf>.
- 560 **6.** Barabási, A.-L. & Oltvai, Z. N. Network biology: understanding the cell's functional organization.
561 Nat. Rev. Genet. **5**, 101–113 (2004).
- 562 **7.** Maslov, S. & Sneppen, K. Specificity and stability in topology of protein networks. Science **296**,
563 910–913, DOI: [10.1126/science.1065103](https://doi.org/10.1126/science.1065103) (2002). [https://science.sciencemag.org/content/296/5569/](https://science.sciencemag.org/content/296/5569/910.full.pdf)
564 [910.full.pdf](https://science.sciencemag.org/content/296/5569/910.full.pdf).

- 565 **8.** Pilosof, S., Porter, M. A., Pascual, M. & Kéfi, S. The multilayer nature of ecological networks.
566 Nat. Ecol. & Evol. **1**, 0101, DOI: [10.1038/s41559-017-0101](https://doi.org/10.1038/s41559-017-0101) (2017).
- 567 **9.** Bullmore, E. & Sporns, O. Complex brain networks: graph theoretical analysis of structural and
568 functional systems. Nat. Rev. Neurosci. **10**, 186–198 (2009).
- 569 **10.** Watts, D. J. & Strogatz, S. H. Collective dynamics of ‘small-world’ networks. Nature **393**, 440–442
570 (1998).
- 571 **11.** Cattuto, C. et al. Dynamics of person-to-person interactions from distributed rfid sensor networks.
572 PLOS ONE **5**, 1–9, DOI: [10.1371/journal.pone.0011596](https://doi.org/10.1371/journal.pone.0011596) (2010).
- 573 **12.** Stehlé, J. et al. High-resolution measurements of face-to-face contact patterns in a primary school.
574 PLOS ONE **6**, 1–13, DOI: [10.1371/journal.pone.0023176](https://doi.org/10.1371/journal.pone.0023176) (2011).
- 575 **13.** Rombach, M. P., Porter, M. A., Fowler, J. H. & Mucha, P. J. Core-periphery structure in networks.
576 SIAM J. on Appl. Math. **74**, 167–190, DOI: [10.1137/120881683](https://doi.org/10.1137/120881683) (2014). [https://doi.org/10.1137/](https://doi.org/10.1137/120881683)
577 [120881683](https://doi.org/10.1137/120881683).
- 578 **14.** Alvarez-Hamelin, J. I., Dall’Asta, L., Barrat, A. & Vespignani, A. K-core decomposition of Internet
579 graphs: hierarchies, self-similarity and measurement biases. Networks and Heterogeneous Media **3**,
580 371 (2008).
- 581 **15.** Kitsak, M. et al. Identification of influential spreaders in complex networks. Nat. Phys. **6**, 888–893
582 (2010).
- 583 **16.** Zhou, S. & Mondragon, R. The rich-club phenomenon in the internet topology. IEEE Commun. Lett.
584 **8**, 180–182 (2004).
- 585 **17.** Colizza, V., Flammini, A., Serrano, M. A. & Vespignani, A. Detecting rich-club ordering in complex
586 networks. Nat. Phys. **2**, 110–115 (2006).
- 587 **18.** Opsahl, T., Colizza, V., Panzarasa, P. & Ramasco, J. J. Prominence and control: The weighted
588 rich-club effect. Phys. Rev. Lett. **101**, 168702, DOI: [10.1103/PhysRevLett.101.168702](https://doi.org/10.1103/PhysRevLett.101.168702) (2008).
- 589 **19.** Serrano, M. A. Rich-club vs rich-multipolarization phenomena in weighted networks. Phys. Rev. E
590 **78**, 026101, DOI: [10.1103/PhysRevE.78.026101](https://doi.org/10.1103/PhysRevE.78.026101) (2008).

- 591 **20.** McAuley, J. J., da Fontoura Costa, L. & Caetano, T. S. Rich-club phenomenon across complex
592 network hierarchies. Appl. Phys. Lett. **91**, 084103, DOI: [10.1063/1.2773951](https://doi.org/10.1063/1.2773951) (2007). [https://doi.org/](https://doi.org/10.1063/1.2773951)
593 [10.1063/1.2773951](https://doi.org/10.1063/1.2773951).
- 594 **21.** van den Heuvel, M. P. & Sporns, O. Rich-club organization of the human connectome. J. Neurosci.
595 **31**, 15775–15786, DOI: [10.1523/JNEUROSCI.3539-11.2011](https://www.jneurosci.org/content/31/44/15775.full.pdf) (2011). [https://www.jneurosci.org/](https://www.jneurosci.org/content/31/44/15775.full.pdf)
596 [content/31/44/15775.full.pdf](https://www.jneurosci.org/content/31/44/15775.full.pdf).
- 597 **22.** Towilson, E. K., Vértés, P. E., Ahnert, S. E., Schafer, W. R. & Bullmore, E. T. The rich club of the c.
598 elegans neuronal connectome. J. Neurosci. **33**, 6380–6387, DOI: [10.1523/JNEUROSCI.3784-12.2013](https://www.jneurosci.org/content/33/15/6380.full.pdf)
599 (2013). <https://www.jneurosci.org/content/33/15/6380.full.pdf>.
- 600 **23.** Nigam, S. et al. Rich-Club Organization in Effective Connectivity among Cortical Neurons.
601 The J. Neurosci. **36**, 670–684 (2016).
- 602 **24.** Holme, P. & Saramäki, J. Temporal networks. Phys. Reports **519**, 97–125 (2012).
- 603 **25.** Holme, P. Modern temporal network theory: a colloquium. The Eur. Phys. J. B **88**, 234 (2015).
- 604 **26.** Holme, P. & Saramäki, J. (eds.) Temporal Network theory (Springer, Singapore, 2019).
- 605 **27.** Braha, D. & Bar-Yam, Y. From centrality to temporary fame: Dynamic centrality in complex networks.
606 Complexity **12**, 59–63, DOI: <https://doi.org/10.1002/cplx.20156> (2006).
- 607 **28.** Braha, D. & Bar-Yam, Y. Time-dependent complex networks: Dynamic centrality, dynamic motifs,
608 and cycles of social interactions. In Gross, T. & Sayama, H. (eds.) Adaptive Networks, vol. 51 of
609 Understanding Complex Systems, 39–50 (Springer Berlin / Heidelberg, 2009).
- 610 **29.** Pedreschi, N. et al. Dynamic core-periphery structure of information sharing networks in entorhinal
611 cortex and hippocampus. Netw. Neurosci. **4**, 946–975 (2020).
- 612 **30.** Braun, U. et al. Dynamic reconfiguration of frontal brain networks during executive cognition in
613 humans. PNAS **112**, 11678–11683 (2015).
- 614 **31.** Pfitzner, R., Scholtes, I., Garas, A., Tessone, C. J. & Schweitzer, F. Betweenness preference:
615 Quantifying correlations in the topological dynamics of temporal networks. Phys. Rev. Lett. **110**,
616 198701, DOI: [10.1103/PhysRevLett.110.198701](https://doi.org/10.1103/PhysRevLett.110.198701) (2013).
- 617 **32.** Scholtes, I., Wider, N. & Garas, A. Higher-order aggregate networks in the analysis of temporal
618 networks: path structures and centralities. Eur. Phys. J. B **89**, 1–15 (2015).

- 619 **33.** Masuda Naoki, M. J. C. & Petter, H. Concurrency measures in the era of temporal network.
620 J. R. Soc. Interface.182021001920210019 (2021).
- 621 **34.** Bajardi, P., Barrat, A., Natale, F., Savini, L. & Colizza, V. Dynamical patterns of cattle trade
622 movements. PloS one **6**, e19869 (2011).
- 623 **35.** Kovanen, L., Karsai, M., Kaski, K., Kertész, J. & Saramäki, J. Temporal motifs in time-dependent
624 networks. J. Stat. Mech. Theory Exp. **2011**, P11005 (2011).
- 625 **36.** Longa, A., Cencetti, G., Lepri, B. & Passerini, A. An efficient procedure for mining egocentric
626 temporal motifs. Data Min. Knowl. Discov. (2021).
- 627 **37.** Galimberti, E., Barrat, A., Bonchi, F., Cattuto, C. & Gullo,
628 F. Mining (maximal) span-cores from temporal networks. In
629 Proceedings of the 27th ACM International Conference on Information and Knowledge Management,
630 107–116 (ACM, 2018).
- 631 **38.** Ciaperoni, M. et al. Relevance of temporal cores for epidemic spread in temporal networks.
632 Sci. Reports **10**, 12529, DOI: [10.1038/s41598-020-69464-3](https://doi.org/10.1038/s41598-020-69464-3) (2020).
- 633 **39.** Zhou, S. & Mondragón, R. Structural constraints in complex networks. New J. Phys. **9**, 173 (2007).
- 634 **40.** Gauvin, L. et al. Randomized reference models for temporal networks (2018). [1806.04032](https://arxiv.org/abs/1806.04032).
- 635 **41.** Masuda, N. & Holme, P. Detecting sequences of system states in temporal networks. Sci. Reports **9**,
636 795 (2019).
- 637 **42.** Valdano, E. et al. Predicting epidemic risk from past temporal contact data. PLOS Comput. Biol. **11**,
638 1–19, DOI: [10.1371/journal.pcbi.1004152](https://doi.org/10.1371/journal.pcbi.1004152) (2015).
- 639 **43.** Gautreau, A., Barrat, A. & Barthélemy, M. Microdynamics in stationary complex networks.
640 Proc. Natl. Acad. Sci. **106**, 8847–8852, DOI: [10.1073/pnas.0811113106](https://doi.org/10.1073/pnas.0811113106) (2009). [https://www.pnas.
641 org/content/106/22/8847.full.pdf](https://www.pnas.org/content/106/22/8847.full.pdf).
- 642 **44.** Salathé, M. et al. A high-resolution human contact network for infectious disease transmission.
643 Proc. Natl. Acad. Sci. **107**, 22020–22025, DOI: [10.1073/pnas.1009094108](https://doi.org/10.1073/pnas.1009094108) (2010).
- 644 **45.** Barrat, A., Cattuto, C., Tozzi, A. E., Vanhems, P. & Voirin, N. Measuring contact patterns with wear-
645 able sensors: methods, data characteristics and applications to data-driven simulations of infectious
646 diseases. Clin. Microbiol. Infect. **20**, 10–16, DOI: [10.1111/1469-0691.12472](https://doi.org/10.1111/1469-0691.12472) (2014).

- 647 **46.** Gelardi, V., Le Bail, D., Barrat, A. & Claidiere, N. From temporal network data to the dynamics
648 of social relationships. Proc. Royal Soc. B: Biol. Sci. **288**, 20211164, DOI: [10.1098/rspb.2021.1164](https://doi.org/10.1098/rspb.2021.1164)
649 (2021).
- 650 **47.** Valdano, E., Poletto, C. & Colizza, V. Infection propagator approach to compute epidemic thresholds
651 on temporal networks: impact of immunity and of limited temporal resolution. The Eur. Phys. J. B
652 **88**, 341 (2015).
- 653 **48.** Valdano, E., Ferreri, L., Poletto, C. & Colizza, V. Analytical computation of the epidemic threshold
654 on temporal networks. Phys. Rev. X **5**, 021005, DOI: [10.1103/PhysRevX.5.021005](https://doi.org/10.1103/PhysRevX.5.021005) (2015).
- 655 **49.** Clawson, W. et al. Computing hubs in the hippocampus and cortex. Sci. advances **5**, eaax4843 (2019).
- 656 **50.** Clawson, W. et al. Disordered information processing dynamics in experimental epilepsy. bioRxiv
657 DOI: [10.1101/2021.02.11.430768](https://doi.org/10.1101/2021.02.11.430768) (2021).
- 658 **51.** Gelardi, V., Fagot, J., Barrat, A. & Claidière, N. Detecting social (in)stability in primates from their
659 temporal co-presence network. Animal Behav. **139**, 239 (2019).
- 660 **52.** Singer, W. Neuronal synchrony: a versatile code for the definition of relations? Neuron **24**, 49–65–
661 111–25 (1999).
- 662 **53.** Hebb, D. O. The organization of behavior: A neuropsychological theory (Psychology Press, 2005).
- 663 **54.** Varela, F., Lachaux, J.-P., Rodriguez, E. & Martinerie, J. The brainweb: phase synchronization and
664 large-scale integration. Nat. reviews neuroscience **2**, 229–239 (2001).
- 665 **55.** Masuda, N. & Holme, P. (eds.) Temporal Network Epidemiology (Springer, Singapore, 2017).
- 666 **56.** Kobayashi, T., Takaguchi, T. & Barrat, A. The structured backbone of temporal social ties.
667 Nat. Commun. **10**, 220 (2019).
- 668 **57.** Hill, S. & Braha, D. Dynamic model of time-dependent complex networks. Phys. Rev. E **82**, 046105
669 (2010).
- 670 **58.** Laurent, G., Saramäki, J. & Karsai, M. From calls to communities: a model for time-varying social
671 networks. The Eur. Phys. J. B **88**, 301 (2015).
- 672 **59.** Markram, H., Gerstner, W. & Sjöström, P. J. Spike-timing-dependent plasticity: a comprehensive
673 overview. Front. synaptic neuroscience **4**, 2 (2012).
- 674 **60.** Buzsáki, G. Neural syntax: cell assemblies, synapsembles, and readers. Neuron **68**, 362–385 (2010).

- 675 **61.** Ikegaya, Y. et al. Synfire chains and cortical songs: temporal modules of cortical activity.
676 Sci. (New York, N.Y.) **304**, 559–564 (2004).
- 677 **62.** Bonifazi, P. et al. GABAergic hub neurons orchestrate synchrony in developing hippocampal networks.
678 Science **326**, 1419–1424 (2009).